ISSN: 2454-9940

INTERNATIONAL JOURNAL OF APPLIED SCIENCE ENGINEERING AND MANAGEMENT

E-Mail :
editor.ijasem@gmail.com
editor@ijasem.org

www.ijasem.org

INTERNATIONAL JOURNAL OF APPLIED SCIENCE ENGINEERING AND MANAGEMENT

ISSN2454-9940www.ijsem.org
Vol 6, Issuse.4 Oct 2018

Research on the similarities and differences between Conditional Source-term Estimation (CSE) and Conditional Moment Closure (CMC) with regards to piloted jet flames

Dr. VeeramalaiSankardass ,Dr. Suresh Kumar

abstract

Direct side-by-side comparison of the Sandia flames is used to examine Conditional Moment Closure (CMC) and Conditional Source-term Estimation (CSE). The purpose of this research is to compare the efficacy of various modeling approaches under similar situations and computational frameworks. We evaluate the accuracy of CMC and CSE predictions against extensive experimental data. In the instance of Sandia flame D, the turbulent flow and mixing fields predicted by CMC and CSE are identical close to the nozzle exit, in accordance with the actual observations, but they diverge farther downstream. Good agreement exists between the experimental results obtained downstream of the nozzle for lean mixtures and the conditional mass fractions calculated using CMC and CSE for the principal species. There are several axial sites for fuel-rich mixes where the conditional mass proportion of methane is underestimated while the conditional mass fraction of water is overestimated. The main features of the experimental profiles are recapitulated by the CMC and CSE conditional mass fractions of the minor species and conditional temperature. However, Sandia flame E is drastically different. It has been determined that RANS, along with boundary conditions established in CMC and certain assumptions made in the chemical tables in CSE, are to blame for the observed differences. Both CMC and CSE Favre-averaged profiles are similar. Time spent running each model in the computer is compared, with CSE coming out on top. Further, some of the benefits and drawbacks of each combustion model are discussed. Results are proven to be of equivalent quality between CMC and CSE when the same numerical techniques, mesh, and boundary conditions are used..

Keywords:CMC Inferno of the CSE SANDIA D type FLAME OF SANDIA E Combustion Turbulence

Introduction

Closure for the mean chemical source term using conditional averaged quantities is provided by Conditional Moment Closure (CMC) [1,2] and Conditional Source-term Estimation (CSE) [3,4]. The underlying assumption of these models is that changes in species mass fractions and temperature (or enthalpy) may be linked to changes in one or more scalars that can be used as conditioning variables. In most standard formulations, only one conditioning variable is taken into account, such as the mixture fraction in non-premixed com-bustion. The thin flame assumption is unnecessary in the CMC or CSE derivation, expanding its application. The conditional response rates are closed to first order in flames that are distant from extinction or igniting [4], since the fluctuations around the conditional averages are minor and can be ignored. In this way, specificthe incorporation of chemistry can be done at little computational cost. As an added bonus, the conditional averages exhibit substantially less spatial variability than their unconditional counterparts. Because of this, conditional averages may be computed using a spatial mesh that is coarser than the grid used to solve unconditional averages.

The concepts underpinning CSE and CMC are similar, but the methods used to calculate the conditional values are somewhat different. The conditional averages in CMC are calculated by resolving transport equations. The species and temperature/enthalpy controlling equations are conditionally averaged on a sample space variable to get the transport equations. The resulting physical space and sample space transport equations are then solved. Some unclosed terms, such the conditional velocity and the conditional scalar dissipation rate, need to be modeled, as will be detailed in Section 2.1. CMC methods have been continuously developed by a number of research groups over the past two decades, and they have shown promising results in modeling a wide variety of turbulent combustion problems employing a variety of fuels in Reynolds Averaged Navier-Stokes (RANS) calculations, such as jet and bluff-body flames [5-7], soot in jet flames [8], autogyration [9,10], hood fires [11,12], spray autoignition [13], and soo In [20], the several uses of CMC are reviewed in detail. However, the closure of the conditional scalar dissipation rate of the progress variable and the extra complexity of a non-conserved conditioning variable provide challenges for CMC implementation for turbulent premixed combustion [21]. There is room for development here. Similarly, advancements in CMC based on two conditioning variables for turbulent partially-premixed combustion or situations with significant extinction or ignition have been restricted [22,23]. To the best of the authors' knowledge, there are no known examples of completely connected, doubly conditioned CMC formulations. Doubly conditioned CMC is more difficult than single conditioned CMC because of the presence of two sets of unclosed words.

Department of cse
drveeramalai1@gmail.com, drsuresh718@gmail.com, drprabhu42@gmail.com,
ISL Engineering College.
International Airport Road, Bandlaguda, Chandrayangutta Hyderabad - 500005 Telangana, India.

CSE advancements, on the other hand, are more recent, build on CMC's capabilities while avoiding the closure of the extra terms included in the CMC transport equations. The conditional averages may be derived by inverting an integral equation, as shown in the first CSE article [3], which uses DNS data for an a priori test. While flamelet decomposition was used in the first iterations of integral inversion [24,25], a regularization approach with tabular precise chemistry is now used. Similar to CMC, CSE was first implemented for non-premixed instances and is continually evolving [24,25,27-31]. Recent years have seen advancements in our understanding of premixed combustion [26,32,33], multi-stream configurations [34,35], and partially-premixed flames [36-38]. In the latter two cases, CSE closes the mean reaction rates without the need for closure of extra and difficult terms by using the utilization of doubly conditionally averaged quantities. Key CSE elements for high performance are precise inversion using a regularization approach [39] and a chemistry table that is realistic of the fuel and the task at hand [30].

As can be seen, CMC and CSE have certain things in common, and each has advantages and disadvantages that may become apparent depending on the context. Both methods have progressed to the point where they can be compared side by side for the same turbulent flame inside the same Computational Fluids Dynamics (CFD) framework, and evaluated for their forecast accuracy, computational time, and potential.

The purpose of this analysis is to compare and contrast the various modeling approaches under identical settings and computational frameworks. We employ the same CFD numerical techniques, mesh, and boundary conditions for both sets of simulations to reduce inconsistencies. In order to provide a fair comparison between CMC and CSE, only RANS simulations are taken into account.

Since the two models are founded on the same fundamental idea, it is crucial to identify and address the factors contributing to the differences in their forecasts. Both conditional mass balance and conditional species equilibria (CMC and CSE) rely on the direct retrieval of the conditional mass fractions of species through the solution of transport equations or inte- gral inversion, respectively. Numerical approximations and inaccuracies are introduced during the integral inversion procedure. No direct comparison with CMC has yet been done to evaluate the magnitude of this inaccuracy. Because of this, it is essential to evaluate whether or not the conditional profiles acquired by CSE through this inversion procedure are equivalent to those derived using the transport equations in CMC. The study presented here is the first to compare and contrast the two models head-to-head. In order to do this, we need well-characterized examples of turbulent flames that have not been premixed. Detailed experimental data on the mean axial velocities, temperatures, Favre-averaged mass fractions, mean mixture fractions, and mixture fraction root mean squares suggest that the Sandia piloted jet flames are a promising contender.

(rms), and some conditional species concentrations at different lo-cations[40].

$$\frac{(N|\eta)}{\tilde{N}} = \int_0$$

$$G(\eta) = \exp\left(-2[erf^{-1}(2\eta-1)^2\right) \quad] \ ,$$

where a is the vector including $(Y_k|\eta)$, b is the vector containing

Many tur- bulent combustion models in RANS and LES have been used to successfully simulate the Sandia flames. These models include a Lagrangianflamelet model [41], a steady flamelet formulation [42], a flamelet model including a progress variable [43], and various Probability Density Function (PDF) approaches [44-50]. As an additional point of reference, the Sandia flames have been used in a number of CMC and CSE research. Good agreement is found for the conditional mass fractions of the principal species and temperature for lean mixtures in RANS when using radially-averaged first order CMC incorporating radiation [7]. Inaccuracies in the chemical kinetics and non-negligible conditional fluctuations in fuel-rich areas explain the discrepancies reported between predictions and experimental evidence for fuel-rich mixes. Kronenburg and Kostka [23] provide a pretabulated dual conditioning approach that takes into account the impact of conditional fluctuations on conditional response rates. Since the primary species in the Sandia flame D do not significantly shift, the disagreement between our study and the findings previously reported by Room- ina and Bilger [7] must arise from differences in chemical kinetics in the fuel-rich zone. While Brizuela and Roudsari [51] do compare their results to experimental data in conditional space, they do do so in a restricted way. Predictions of species mass fractions are demonstrated to be enhanced by using second order CMC [52] and a second order La- grangian CMC approach [53]. When utilizing second order CMC, however, we do not see any increase in extinction. Better spatial and temporal resolu- tion of turbulent mixing in LES is demonstrated to allow for first order CMC to offer additional improvement compared to previous RANS predictions [54]. The LES-CMC grid sensitivity study [55] confirms this as well. Two different formulations have been used to simulate the Sandia flame D in the context of CSE. First using CSE in LES with a two-step chemical mechanism, Steiner and Bushe [56] found that their predictions were generally in line with the available experimental data. Later, a more refined CSE formulation is investigated, complete with tabu- lated chemistry; the resulting temperature and species concentration values are shown to be in excellent agreement with the experimental results [28]. No published CSE findings on the Sandia E and F flames have been found, as far as the authors are aware.

The current study's implementations of CMC and CSE are detailed below. The major goal is to directly contrast the predictions made by the various formulations. Furthermore, experimental data are provided as a reference point against which the two simulations may be evaluated.

.

Previous CSE research has relied on existing knowledge about the flame to guide the selection of CSE ensembles. It is typical practice in premixed CSE to pick a single ensemble that accounts for the whole domain [26,32]. To take advantage of the modest radial dependency of the conditional averages [4] in non-premixed CSE, the ensembles are often chosen to be planes in the axial direction [27,28]. Two-mixture fraction CSE formulations [34,35] and partly premixed CSE [36] have also benefited from this strategy.

It is possible to discretize Eq. (7) and express it as a matrix:

$$\frac{G(\eta)}{\int \tilde{P}(\eta)G(\eta)d\eta}$$

$$A.\vec{a} = \vec{b},$$

where N is the scalar dissipation rate under all conditions. Using the PDF as an approximation, we may get the PDF of the mixture fraction [59]. According to the gradient diffusion hypothesis, the turbulence fluxes are modeled by the equations (urrYrr |) = DtQk and (urrTrr |) = Dt QT. The mixed fraction conditional probability density function (bin). The difficulty in finding a solution to Eq. (8) stems from the fact that it is ill-posed and sensitive to even minor changes in the system [60]. A regularization strategy is necessary to address this issue. right now

The first order closure is used to simulate the chemical source term $\dot{\omega}_k$.

Estimation of the Source Term Under Conditions 1.1 (CSE)

1.1.1. Principle

As with CMC, CSE was first suggested by Bushe and Steiner [3]. The conditional

approach since it has been shown effective in prior CSE investigations [27,32,35]. Although further regularization techniques exist (see [39]), they are not taken into account here. When used as a regularization method, zeroth-order Tikhonov yields the following enhanced matrix,

$$\vec{a} = \operatorname{argmin} \left\| \vec{A}\vec{a} - \vec{b} \right\|_2^2 + \lambda \left\| \vec{a} - \vec{a}^0 \right\|_2^2 \quad (9)$$

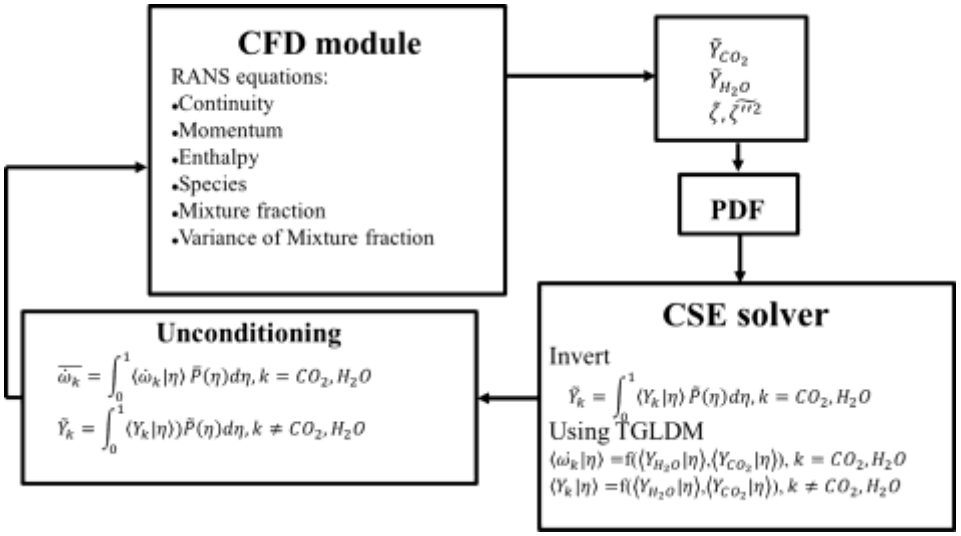

Fig.1. CSEcodestructure.

where $||.||_2$ denotes the L2-norm of a vector, $\vec{a}^0$ the solution from the previous time step, and λ the regularization parameter. In a previous CSE study [36], it was found that the initial choice of $\vec{a}^0$ did not impact the final solution as long as the initial choice was chosen such that the simulation produced a stable flame. The reg-ularization parameter λ is determined by

nal CMC predictions [15]. The same implementation is kept in the current RANS calculations. The CSDR is calculated directly on the CMC mesh using Eq. (5). In CMC, the unconditional values are re-trived by solving Eq.(7).

In both CMC and CSE, transport equations for mean mixture fraction $\tilde{\xi}$ and variance $\widetilde{\xi''^2}$ are resolved. Closure for the turbulent Schmidt number which is set to 0.7.

ferent values of η. Further details on the TGLDM method for non-premixed combustion can be found in [27].

1.1. Summary of equations solved in CMC and CSE

The combustion models CSE and CMC are available in OpenFOAM 2.3 CFD code [62]. When comparing CMC with CSE simulations, you'll find no differences in the boundary conditions, turbulence mo
chemical process. In Sectio
turbulence model, boundar
process used in the numeric
the combustion model ac
predictions, this research p
compare the two models. Fi
the CMC and CSE programs'
The RANS-CMC technique use
different computational mesh
the CMC. Given that conditio
across longer time periods t
understandable. It is necessar

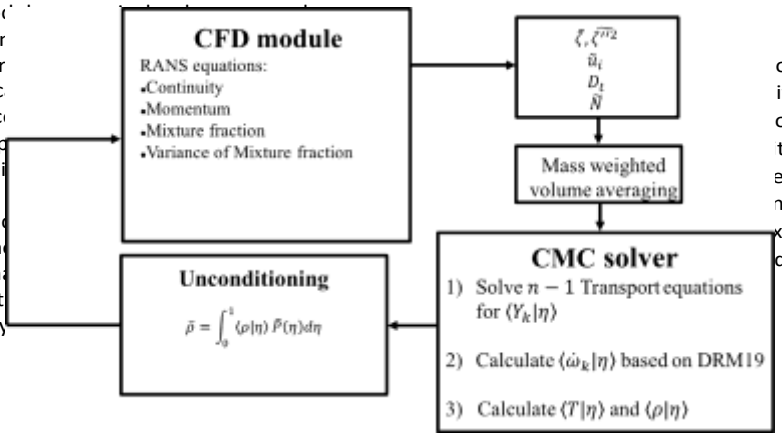

the flow and mixing field from the coarser RANS-CFD resolution to the finer CMC resolution. By averaging over a large volume of data, we can calculate the conditional velocity, turbulent diffusivity, and unconditional scalar dissipation rate [63]. Previous LES-CMC implementations have discovered that mass weighted and PDF weighted averages are both appropriate, with only minor changes in the fi-

Experimental conditions

Since extensive experimental data is available, the methane/air non-premixed piloted Sandia flames examined by Barlow and Frank [40] are chosen for this investigation. A 7.2 mm primary fuel jet and an 18.2 mm pilot are at the heart of the Sandia flames, which are located in a wind tunnel with a 0.9 m/s coflow of air. With a stoichiometric mixture fraction of 0.351, the primary fuel jet consists of 25% methane (CH4) and 75% air by volume. At an equivalency ratio of 0.77, the pilot is a lean combination of ethyne (C2 H2), hydrogen (H2), air, carbon dioxide (CO2), and ni- trogen (N2). The primary jet of the Sandia flame D has a bulk velocity of 49.6 m/s (2 m/s), which corresponds to a Reynolds number of 22,400; the pilot's velocity is 11.4 m/s (0.5 m/s), which is the subject of the current investigation. An even more impressive quantity of local extinctions have been attributed to the Sandia flame E, which has a Reynolds number of 33,600.

on of species, mixture fraction,
ifferent axial positions have been
onal profiles of the mass fractions
tions are also accessible. Raman-
e used to get temperature, species,
n from experiments. Nitrogen (N2),
xide (CO2), hydrogen (H2), carbon
de (OH) all have experimental

Fig. 2. CMC code structure.

2. Computationaldetails

OpenFoam 2.3 [62] is a finite volume programme that uses the CSE and CMC models under the low Ma number assumption. Standard OpenFoam release com- bustion solvers use a PIMPLE pressure correction technique to solve the velocity field. In simulation, the time step may be changed. You may expect a maximum Courant number of 0.3.

CSE uses an integral inversion to calculate conditional averages, while CMC uses the solution of transport equations. Therefore, CMC and CSE need separate numerical methods. In order to solve problems involving finite differences, the CMC code [15,63] was developed. First and second order accurate total variation diminishing (TVD) schemes [64] are used to discretize the convective transport in Eqs. (1) and (2). Mixture fraction and physical space diffusion terms are discretized using a second-order accurate central difference technique. When the size of the system that needs to be solved concurrently is reduced, the computational burden is also reduced, and this is achieved via the use of full operator splitting. The system of ODEs for both the stiff and non-stiff portion of Eqs. (1) and (2) have been integrated using the solver VODPK [65]. (2). Adding transport equations for mixture percent and its variance, the present CSE algorithm is an expansion of the reactingFOAM combustion model. Both CMC and CSE use OpenFOAM's in-built numerical techniques to discretize these transport equations. As part of the inversion procedure, LU decomposition is used to get the solution to Equation (9).

In the current investigation, the computational domain is a small-angle wedge (=5) with a radius of 21D and a height of 100D, where D is the fuel intake diameter equal to 7.2 mm. A two-dimensional object is constructed from a single cell in the direction of the arrow.

simulation. The nozzle areas are represented by a non-uniform grid in which the cell density is greater. The present mesh, consisting of 51,000 cells, has been proved to yield grid independent results after a succession of ever finer meshes were examined.

For the turbulent flow field, this study makes use of the k model [66]. The C1 constant is adjusted, as is customary in the k model, such that it agrees with the velocity estimates from experiments. Using a sensitivity analysis, we found that C1 = 1.52 provides the greatest fit to the data from the experiments. CMC and CSE simulations of methane/air combustion with 19 species and 84 reactions are accompanied by detailed kinetics utilizing the DRM19 mechanism [67]. Boundary conditions for velocities, temperatures, mixture fractions, turbulent kinetic energies, andBoth the kinetic energy k and the dissipation rate of k are chosen to correspond with the range of obtainable experimental circumstances. For the pilot flow, the species mass fraction of CO2 and H2O are both adjusted to their equilibrium compositional values of 0.109 and 0.10006 at the boundary conditions, respectively [51].

Except for pressure, all other fields are constrained by an OpenFOAMzeroGradient boundary condition at the outlet. The outlet pressure boundary condition is set to 0.993 atm [40] while the jet, pilot, and coflow inlet pressure boundary conditions are all set to zeroGradient. Using the Sandia data set and an integral length scale of 1.4 mm, [68] the velocities, turbulent kinetic energies, and turbulent dissipation rates at the jet, pilot, and coflow inlets are determined. For the velocities k and, the intake profiles are discretized along the 30 cells of the pilot and the jet. The possible values of the mixture fraction are discretized into

There are more data points clustered close to the stoichiometric mixture fraction than in any of the other 60 bins. There was very little variation in the predictions while doing simulations with a larger number of bins (90). In this way, we can say that the simulations do not rely on the degree of resolution in the space of mixture fractions. The conditional species mass fractions in CMC are based on a burning flamelet profile at the intake nodes. Mixed boundary conditions for CMC (burning in pilot, inert everywhere else) are not conceivable because of the small number of cells in the radial direction. When using a delta function mixture fraction PDF with the coflow, pilot, and fuel mass fractions of 0, 0.27, and 1, respectively, the flamelet profiles are defined in a way that preserves the right unconditional boundary values.

Setting the conditional mass fraction of CO2 and H2O profiles to generate high reaction rates from the TGLDM tables is the starting point for the CSE calculations. When the concentrations of YCO2 and YH2 O are not high enough to sustain combustion, the startup procedure is stopped. After this is done, the inversion yields the values for (YCO2 |) and YH2 O.

Based on prior CSE research into non-premixed jet flames [27,34,35], 19 ensembles are defined as axial slices of the computational domain, making up a 19x1 CSE grid for the CSE simulations. It has been shown that CSE ensembles are not uniformly distributed, with a larger concentration towards the nozzle exit, where substantial changes to the mixture fraction are anticipated. In contrast, a 25x5 CMC grid is used in the CMC simulations. Thus, in the axial direction, the two simulations have the same spatial resolution, but in the radial direction, the CSE simulations assume the conditional averages stay constant. When comparing the CSE findings to the experimental data, a coarser CMC grid was tried and was shown to provide bigger disparities. Since it is well-known that the accuracy of CMC decreases when the number of cells is decreased, it is not practical to employ a coarser CMC grid in this case.*SandiaflameD*

Fig. 3. Temperature contours with a schematic of the CSE ensembles (left) and CMCgrid(right)superimposed.

presently existing circumstances. Unlike the CMC grid, the CSE grid must have a sufficient number of re- acting cells for the inversion process, hence it could not be manufactured as fine as the CMC grid. Increasing the resolution of the CFD mesh and hence the number of reactive cells in the en- sembles is required for this. In comparison, CMC may use a grid with the same precision as CFD. Still, the CMC transport equations can't be solved without taking into account the large number of CMC cells that reside in the coflowing air. Considering the lack of fuel and chemical processes, CSE excludes these cells from the inversion process. As a consequence, it is not anticipated nor essential that the CMC and CSE grids be equal in order to get comparable quality results. As shown in Fig. 3, the CSE ensembles and CMC grid are depicted in a schematic form.

3. Results

The findings of the simulations of the Sandia flames are broken down into four categories for examination. It begins with a comprehensive breakdown of the Flame D simulation findings. The available experimental data at six axial points is first compared to the Favre-averaged velocity, mixture percent, and its root mean square (rms) generated from the CSE and CMC simulations. The conditional temperature, conditional mass fractions of CO2, H2O, CH4, H2, and OH, and experimental profiles at the same six axial positions are then compared. Although experimental data exists for a wider range of species, only a representative sample was included in this analysis. We may draw the same conclusions about other animals. Following this is a comparison of the Favre-averaged mass fractions and temperatures. Next, the Flame E findings are shown, with special attention paid to the area just next to the nozzle, where the CMC and CSE values diverge. For reasons that will be detailed below, neither model, in its present configuration, was able to provide satisfactory findings for Sandia flame F. Finally, the computational cost of CSE and CMC are compared and contrasted, and the benefits and drawbacks of each method are discussed.

The 5.1.1 Field of Turbulent Flow

As shown in Fig. 4, the axial velocity derived from the CMC and CSE simulations agrees well with the actual data at six axial locations. The agreement between CMC, CSE, and the experimental data is excellent, with all values falling within 3 m/s of each other extremely near to the nozzle at y/D = 3. Further downstream at y/D = 15, the velocities predicted by CMC and CSE for radial locations between r/D = 1 and r/D = 2 are somewhat overpredicted compared to the observed profile. The centerline velocities generated from both the CMC and CSE simulations are around 16% greater than the value measured empirically at y/D = 30. The CMC and CSE estimated velocities off-axis accord well with the experiments. The first three axial points show a remarkable degree of agreement between the two numerical profiles.

distinct from one another. Greater discrepancies in velocity between the CMC and CSE models are shown farther downstream, at y/D = 45 and y/D = 60. Specifically, the centerline experimental velocity is overestimated by around 20% when CSE is applied at y/D = 45.

CMC's estimate for the centerline velocity is around 12% greater than the value derived through experiments. At y/D = 60, a similar pattern is observed: the center-line velocity calculated using CSE is 3 m/s higher than the actual data, but the velocity obtained using CMC is only around 2 m/s higher. Since the identical numbers for velocity, k, and are applied to both CMC and CSE, the discrepancies in the anticipated velocity profiles cannot be explained by changes in the simulations' boundary conditions. Instead, as demonstrated in Section 5.1.5, the divergences in the velocity field may be traced back to discrepancies in the temperature profiles produced by CMC and CSE. Any change in the temperature profiles will cause a change in the jet's spreading rate due to changes in density, k, and. In spite of these minor deviations, the present velocity estimates agree with those of earlier numerical studies for the identical flame [7,55,69]. At this point, it is safe to say that both simulations produce a turbulent flow-field that is consistent with experimental results.

5.1.2 Field of turbulent mixing

The conditional species mass fraction is determined using the mixture fraction probability density function (PDF) in CMC and CSE. So, it's crucial that both CSE and CMC provide accurate predictions of the mean mixture fraction and its rms. In Figs. 5 and 6, we compare the mean mixture percent and its rms field from the CMC and CSE simulations to the experimental results at the same six axial sites.

Figure 5 displays the results for the values of y/D equal to 3, 15, and 30.

CMC and CSE projected mixture fraction profiles are consistent with experimental results. At y/D = 45, farther downstream, more striking variations emerge. Here, CSE's profile shape more closely matches experimental results, but CMC's peak profile fraction prediction is more accurate. The CMC findings reveal a greater overpre- prediction of the mixture fraction profile compared to the CSE predictions between radial sites r/D = 2 and r/D = 5. Within 10%, the CSE predictions and the experimental profile correspond well at the final axial site (y/D = 60). The CMC values are likewise in excellent agreement with the experimental profile here, although they overpredict the mixture percent at radial positions between r/D = 2.5 and r/D = 7.

Several variants in the combination frac-

differences in tionrms between the two groups of numerical simulations. rms profiles from CMC and CSE are similar to one another close to the center.

correspond very closely throughout the whole axis. The experimental root-mean-square (rms) values between r/D = 1 and y/D = 3 are overpredicted by both CMC and CSE.0.5

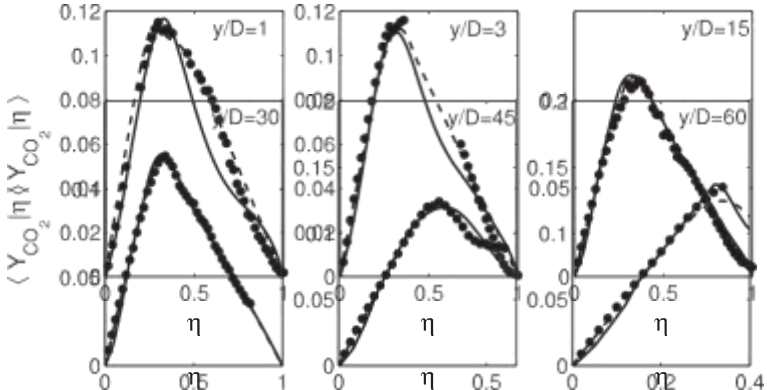

Fig.7. CSE(solidlines)andCMC(dashedlines)conditionalCO_2massfractionprofilescomparedtotheexperimentaldata[40](symbols)atdifferentaxiallocations.

should be exactly the same since they have the same principles in common. However, due to the fact that the conditional averages are generated using different methods—matrix inversion for CSE and transport equations for CMC—each model involves its own set of assumptions, modeling, and numerical mistakes. For this reason, it's possible to see deviations from the projected conditional mass fractions. The CO2 and H2O conditional mass fractions computed by CMC and CSE are first compared to the available experimental data [40] in Figs. 7 and 8.

The CSE simulations rely heavily on the conditional mass fractions of CO2 and H2O, which are retrieved together with the conditional mass fractions of the other species and the conditional temperature from the TGLDM tables, making accurate predictions of these quantities vital. As can be observed in Fig. 7, CSE does a decent job of predicting the conditional mass fraction of CO2 at y/D = 1 and y/D = 3, as compared to the experimental profiles.

Very excellent agreement with the trials is shown between = 0 and = 0.5 in these spots. Under-predictions of about 25% are seen for values between 0.5 and 0.77.

dtotheexperimentaldata[40](symbols)atdifferentaxiallocations.

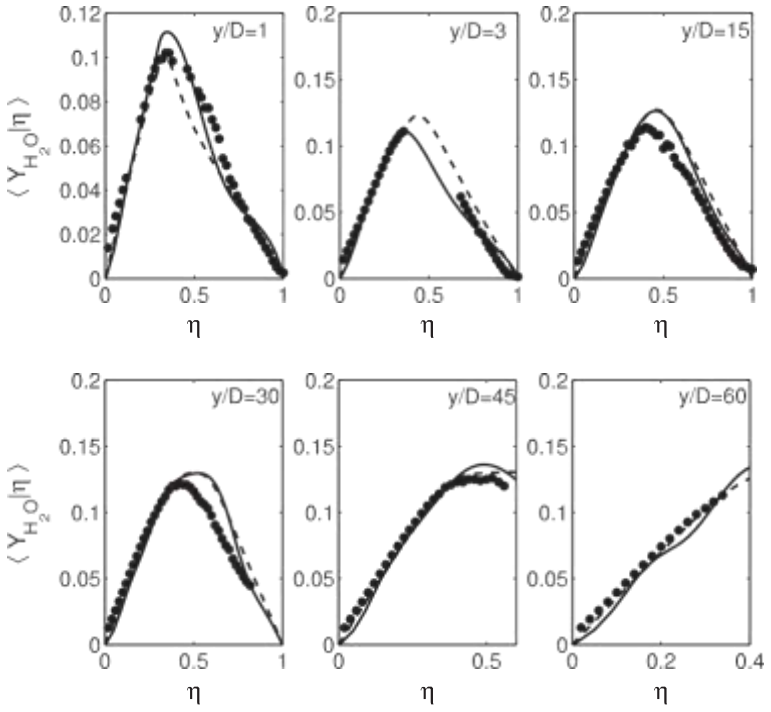

Fig.8.
CSE(solidlines)andCMC(dashedlines)conditionalH_2Omassfractionprofilescompare

calculations of YCO2 using CSE, with the exception of the case when the value of YCO2 is larger than what is seen experimentally (0.7). Mistakes in the predicted mixture fraction rms profiles, which would have an effect on the PDF, may be to blame for the disparities between CSE and the experimental results at these sites. At y/D = 1, the CSE and experimental numbers differ by around 2% from the CMC predictions, which reveal a peak in the conditional CO2 mass fractions. While CMC and CSE profiles agree within 11% for lean mixes, CMC does a better job of capturing the conditional profiles for > 0.5, with an underprediction of just 5% compared to 33% when using CSE at =0.6 and y/D = 1. CSE and the experimental data have agreed extremely well over the last y/D = 3, with the largest discrepancy being about 2% at y/D = 15 for = 0.31. These are areas of very low population density, where

Both CMC and CSE have their own unique characteristics. Therefore, the CMC and CSE predictions are quite near to each other at places far from the nozzle where the boundary conditions do not affect the expected conditional averages. This convergence is encouraging since the conditional averages are determined by two unique approaches. This also shows that the conditional averages can be reproduced accurately by the inversion process employed in CSE without the usage of a submodel.

Figure 8 shows that similar patterns may be seen for the conditional mass fraction of H2O derived from CSE as it is close to the nozzle. Good agreement is shown at y/D = 1 and y/D = 3, but the peak of YH2 O is underestimated by around 10% at y/D = 1. With respect to lean mixes, the CMC findings match well with the CSE and experimental data at the same sites, to within around 10%. However, the H2O conditional mass frac- tions determined from CMC are almost 24% lower than the experimental values for rich mixes (0.36). It is possible that the inconsistencies in the YH2 O profiles at y/D = 1 and y/D = 3 compared to the predictions of (YCO2 |) are attributable to the choice of boundary conditions in CMC at the pilot boundary. At axial coordinates y/D = 5 and outward, Roomina and Bilger [7] detail the adiabatic equilibrium compositions of all reactive scalars except nitric ox- ides (NO). It is claimed that this approximation has little effect on downstream places. The

The present study's CMC findings corroborate this finding.

When extrapolated to downstream regions, the CSE and CMC profiles are quite similar to one another, with a discrepancy of just 0.01 between them and the experimental data for 0.35. Comparatively, the conditional mass fraction of H2O is more than the experimental value for rich mixes with 0.37 0.77. The study of Roomina and Bilger [7] at y/D = 30 utilizing a wide range of chemical processes, including GRI 2.11[70], shows a similar pattern, with (YCO2 |) for rich mixes being appropriately predicted but (YH2 O|) being overestimated. For all axial sites beyond y/D = 3, CMC and CSE agree, proving that the inversion method used in CSE produces the same conditional profiles as CMC.

Figure 9 shows that the CSE and CMC conditional mass fraction of CH4 closely tracks the experimental profile at y/D = 1 and y/D = 3. Since the primary com- bustion products, (YCO2 |) and (YH2 O|), are well predicted (Figs. 7 and 8), the strong agreement revealed by CSE and CMC at these sites for fuel lean mixes is to be anticipated. The increased conditional mass fractions of H2O found for fuel rich mixes in both sets of simulations are reflected in the CMC and CSE profiles that are near to and below the actual values for 0.5 at y/D = 15 and y/D = 30, as shown in Fig. 8. As is shown in the CMC findings of Roomina and Bilger [7], the conditional re- action rates of CH4 are overpredicted for fuel rich combinations in most flame areas.

FIGURE 10: The H2 mass fraction under various conditions. H2 has a higher disparity between the conditional mass fractions predicted by CSE and CMC compared to CO2, H2O, and CH4. Both the CSE and the CMC pro-files shrink down at y/D = 1, whereas the experimental profile remains quite wide. Both CMC and CSE overestimate the peak conditional mass fractions of H2 at this point, however CSE does a somewhat better job of forecasting where this peak will be in the context of the total mixture fraction. The H2 values for rich mixture fractions are underestimated by CSE, although the CMC and CSE agree well for lean mixture fractions at downstream y/D = 3. CMC and CSE forecasts at y/D = 15 accord rather well with the experimental profile. Farther

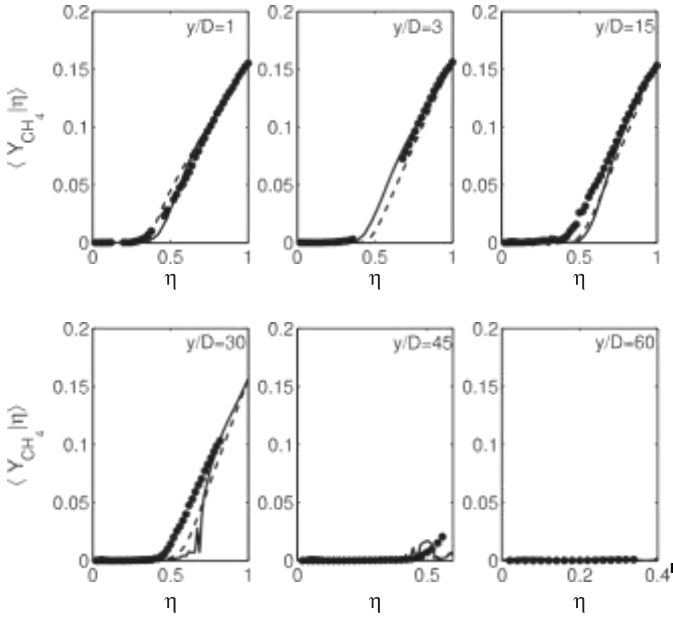

Fig. 9. CSE (solid lines) and CMC (dashed lines) conditional CH_4 mass fraction pro-filescomparedtotheexperimentaldata[40](symbols)atdifferentaxiallocations.

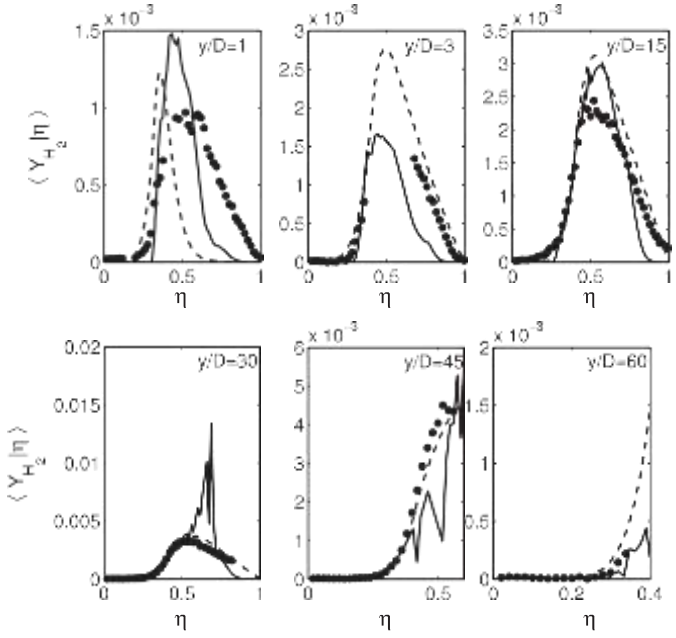

Fig. 10. CSE (solid lines) and CMC (dashed lines) conditional H_2 mass fraction pro-filescomparedtotheexperimentaldata[40](symbols)atdifferentaxiallocations.

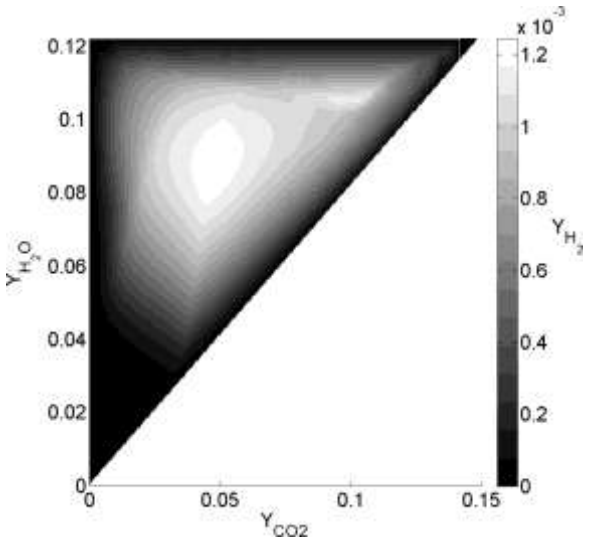

Fig.11. Y_{H_2} massfractionfromTGLDMtableatη=0.3478.

The CMC values at y/D = 30 and y/D = 45 downstream are consistent with the experimental data. The same holds true for the y/D = 30 case with 0.5 CSE predictions. The angular CSE profile is noteworthy, and it can be seen at y/D = 45 and y/D = 60 as well. The interpolations in the TGLDM tables that make use of the convergent conditional CO2 and H2O profiles are the root cause of these shattered CSE profiles, not the lack of convergence in the CSE solution. One of the drawbacks of the current chemical tabulation approach adopted for CSE may be seen in these broken profiles. A mass fraction of H2 inside the TGLDM manifold at = 0.3478 is shown in Fig. 11.

When looking at the TGLDM tables, keep in mind that YH2 = 0 is the initial boundary condition for all trajectories. Figure 11 shows that, as expected

The mass fraction of H2 at the manifold's boundaries is 0 as a consequence of this approximation. As a result, the profile of YH2 observed in Fig. 10 may be seen towards the edge of the TGLDM tables due to the presence of high gradients. CSE-TGLDM for a sequence of methanol flames has been the subject of a similar observation [30]. The conditional mass fractions of YH2 at an axis height of y/D = 30 are larger than the experimental values for rich mixes. Figure 7 shows that the projected conditional mass fraction of CO2 is in line with the actual results, but the expected value of YH2 O is almost 30% higher. Higher H2 levels are exhibited in Fig. 10 because the present CSE and CMC simulations overestimate the consumption of methane (CH4) and oxygen (O2) for these values of. CMC findings are more consistent and accurate in capturing the conditional mass fraction for both lean and rich mixtures, with smoother profiles. Also, unlike CSE, CMC does not grossly overpredict the conditional mass fraction of H2 for rich mixes at y/D = 30. Due to the low PDF values seen in rich combinations, the discontinuities in the CSE profiles observed in these mixtures will be smoothed out in the Favre-

averaged profiles, as will be demonstrated in Section 5.1.5.

The present study's focus is on the YOH| conditional mass fraction. Figure 12 shows that both CMC and CSE successfully capture the highest position of conditional OH mass fraction at y/D = 1. CSE, however, overestimates the peak's amplitude by around 65%, whereas CMC is within 2% of the actual value. The anticipated conditional mass fraction of OH derived from CSE near the nozzle has the highest discrepancy when compared to the experimental data, as is the case for the other minor species. Both rich and lean mixes grossly underestimate the conditional mass fraction of OH at these sites (y/D = 1 and y/D = 3). Similarly to YH2 , the boundary constraints imposed on YOH at the manifold's borders cause the discontinuities seen in the conditional profiles. On the other hand, the CMC findings more accurately reproduce the breadth of the (YOH|) across all axial positions. We suspect that the proximity of the results to the table borders where the OH concentration is set to zero for the chemical tabulation accounts for the excellent agreement seen for CSE at y/D = 60. As a result, the lower OH values achieved by interpolation would be attributable to interpolation rather than a fundamental improvement of the CSE model as compared to CMC. As a result, better approximating the mass fractions of minor species in CSE would benefit from enhancements to the present TGLDM boundary conditions.

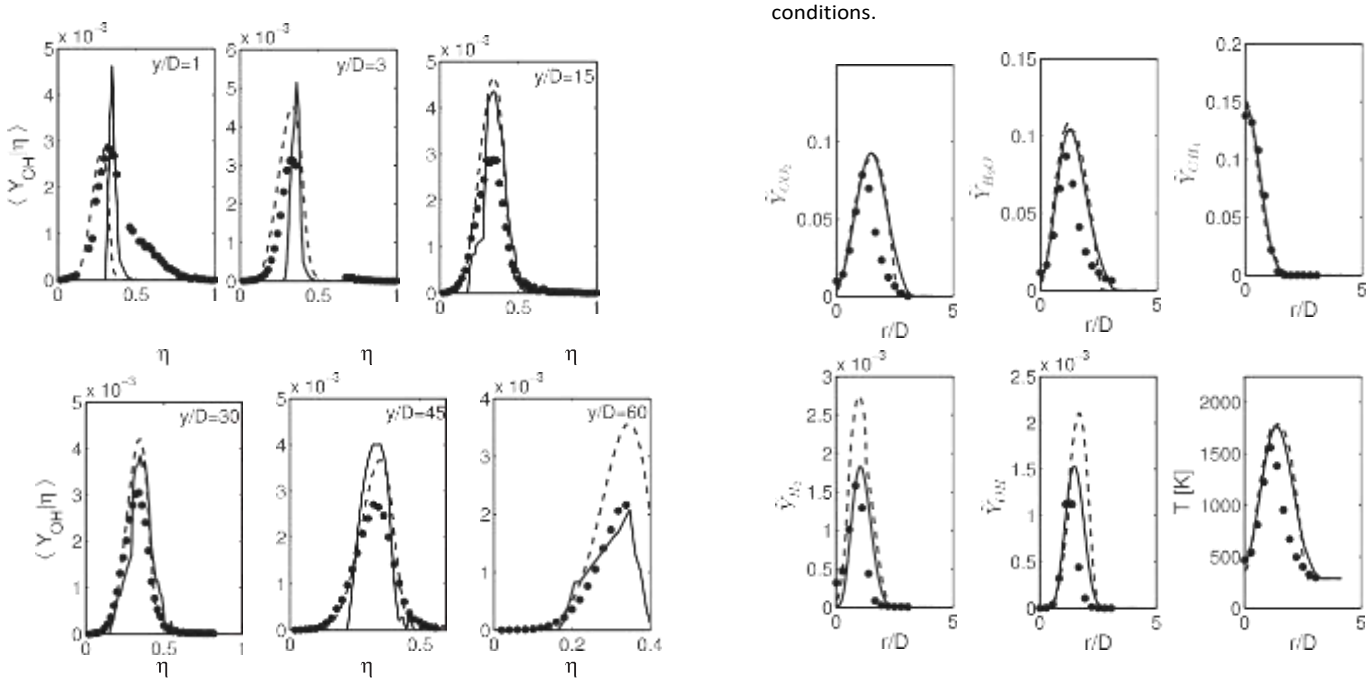

Fig.12. CSE(solidlines)andCMC(dashedlines)conditionalOHmassfractionpro-filescomparedtotheexperimentaldata[40](symbols)atdifferentaxiallocations.

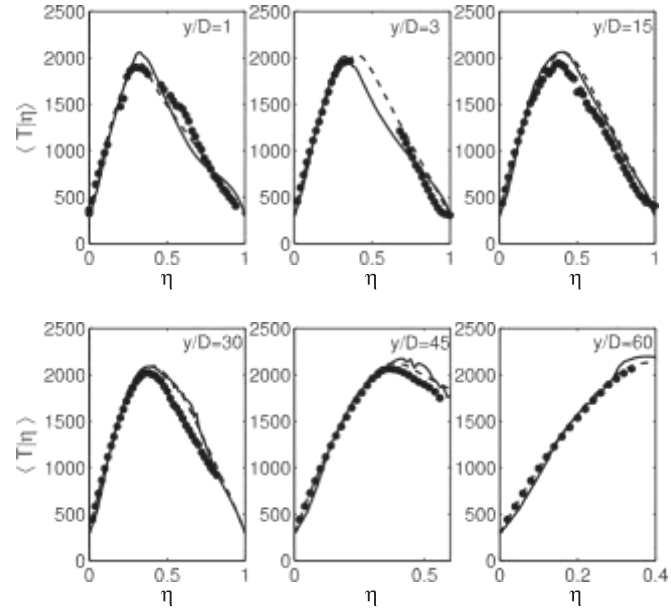

Fig.13. CSE(solidlines)andCMC(dashedlines)conditionaltemperatureprofilescomparedtotheexperimentaldata[40](symbols)atdifferentaxiallocations.

TheoverpredictionofOHinCMCisalsoobservedinLES-CMCsim-ulationsof[55]andmaybeduetochemicalmechanismused.

5.1.3. Conditionaltemperature

In Fig. 13, we see the CSE and CMC findings alongside the experimental conditional temperature patterns. Figure 13 shows that both the CSE and CMC simulations provide accurate predictions about the overall shape of the conditional temperature. For the most part, the peak temperature agrees with the experimental results, although only marginally. High temperatures seen in the CMC and CSE simulations may be due to the exclusion of radiation from the present investigation. At the nozzle's tip, the CSE and CMC diverge somewhat. The peak temperature predicted by CSE is around 8% higher than the experimental and situated at y/D = 1.

Figure 14: Radial temperature and Favre-averaged species profiles for CSE (solid lines) and CMC (dashed lines) compared to the experimental data [40] (symbols) at y/D = 15.

little below the CMC profile's ideal blend fraction. Maximum temperatures predicted by CSE and CMC vary by around 5% at this site. A higher peak temperature at a slightly greater mixing percent is seen for CMC when y/D = 3. The predicted temperatures from both CMC and CSE are within 100 K of each other away from the nozzle, which is in keeping with the excellent predictions shown in Figs. 7 and 8 for the principal product species, and is also in good agreement with the experimental profiles.

Estimates based on Favre's averages 5.1.4

Good agreement is established between the projected conditional mass fraction of main species and the conditional temperatures and the experimental results. However, significant variations in YH2 and YOH| are seen. To assess how these deviations affect the unconditional Favre-averaged quantities is the goal of this section. For this analysis, we compare the flame at three different axial locations: y/D = 15, y/D = 30, and y/D = 45.

Fig. 14 displays a comparison between the experimental data and the Favre-averaged mass fractions of CO2, H2O, CH4, H2, and OH derived from CMC and CSE for y/D = 15. If you look at Fig. 14, you'll find that for r/D = 1.5, the Favre-averaged mass fraction of the main species determined from CMC and CSE agree within a margin of error of less than 0.01. This concordance makes sense, given that both combustion models anticipated comparable conditional profiles for these species. CMC and CSE predictions are in good agreement with experimental pro- files at the centerline, but are noticeably higher for radial locations greater than 2D. This may be because of the overprediction of the mean mixture percentage and its variance, as seen in Figs. 5 and 6, which may be attributable to the fact that radiation was overlooked throughout the computations. Both CMC and CSE overestimate the experimental peak for the mean mass fraction of H2 by 73% and 13%, respectively. This is to be anticipated given the overprediction in the conditional profiles, as seen in Fig. 10. In the same vein, the conditional profile trends are supported by the CMC and CSE, which both provide peak YOH levels that are around 72% and 36% greater than the experimental value (Fig. 12).

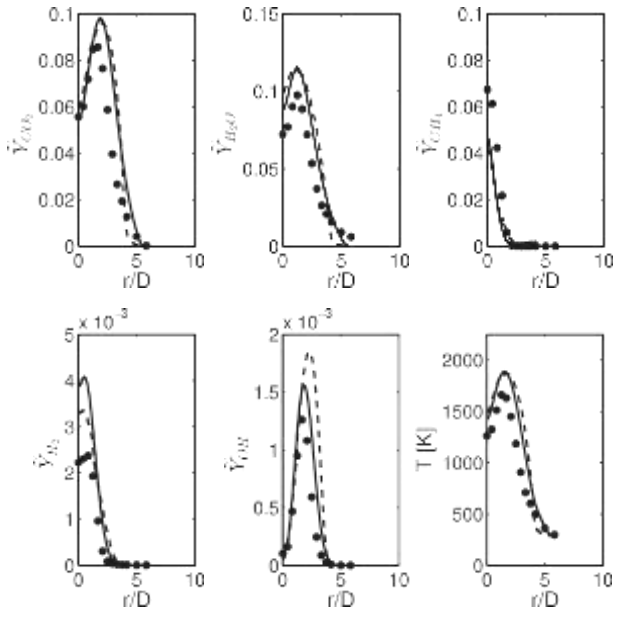

Fig.15.CSE(solidlines)andCMC(dashedlines)radialtemperatureandFavre-averagedspeciesprofilescompared to the experimental data [40](symbols) at*y/D*=30.

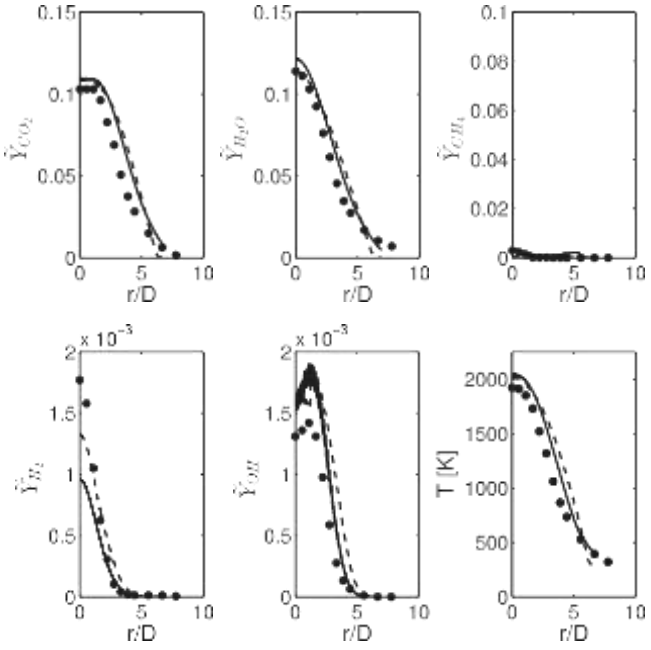

Fig.16.CSE(solidlines)andCMC(dashedlines)radialtemperatureandFavre-averagedspeciesprofilescompared to the experimental data [40](symbols) at*y/D*=45.

Favre-averaged forecast temperatures trend in the same direction as those for the main taxa. Favre-averaged mass fractions and unconditional temperatures retrieved from the CMC and CSE simulations are compared to the experimental data in Figs. 15 and 16.

The CMC and CSE profiles show the same general tendencies as stated for y/D = 15 at y/D = 30. Consistent with the findings for the conditional profiles, the CMC and CSE values are extremely near to one another, frequently being indistinguishable. However, the conditional mass fractions of H2 obtained by CSE are much lower than the CMC

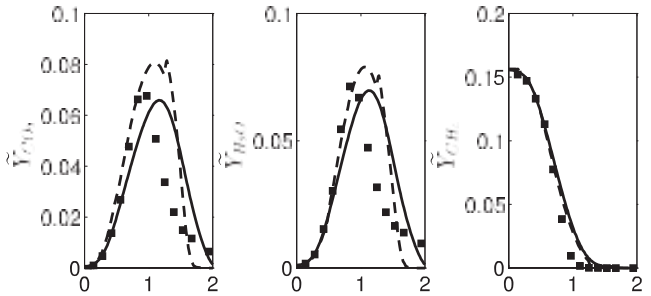

values, making it intriguing to compare the two sets of data.

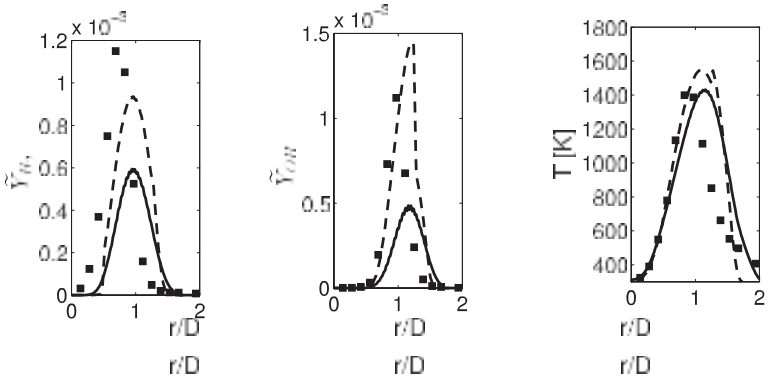

Fig.17.CSE(solidlines)andCMC(dashedlines)radialtemperatureandFavre-averagedspeciesprofilescompared to the experimental data [40](symbols) at*y*/*D*=7.5fortheSandiaEflame.

When compared to CMC and experimental data, this resulted in an overprediction of rich combinations. Having higher CSE values of YH2 for rich mixtures isn't going to change the results of the unconditional mass fraction analysis, as this demonstrates. The largest gap is found to be between 39 and 73% when comparing the peak YH2 between the CMC and CSE simulations with the observed values.

differences between numerical results and experimental data.
Similar patterns emerge at y/D = 45 for the Favre-averaged mass percentage of species and the unconditional temperature. When comparing the two combustion models, the Favre-averaged mass fractions of the main species and the temperature (shown in Fig. 16) are quite similar.

Similar to upstream locations, minor species YH2 and YOH exhibit the largest differences in abundance across the two combustion models.
Curiously, the values of YOH at the centerline and the peak are overestimated by CSE and CMC by around 26 and 33%, respectively. When compared to experimental data, CMC's prediction for the peak value of YH2 is 25% lower, demonstrating better agreement with the facts.

Sandia 5.1's E-flame

Temperature and species mass fraction profiles for the Sandia flame E in both ideal and realistic circumstances are shown in Figs. 17 and 18, respectively. Reduced temperature and OH levels are indicative of the flame's extinction, which peaks at y/D = 7.5. This study's CMC is unable to identify the pattern since RANS almost eliminates localized extinction. In this study, simulating using a mixed inlet boundary condition (burning in pilot, non-reacting everywhere else) did not lead to more accurate predictions from the CMC (not shown). Using mixed inlet boundary conditions for the Sandia D and E flames, as in the previous RANS-CMC simulations [52,53], led to an overestimation of Flame E's temperature. According to the findings shown in [55], which are based on LES-CMC simulations of Flame F, this tendency may be accurately captured by the method. Significant elements in LES-CMC include time-varying velocity variations and mixed inlet boundary conditions. simulations of the Sandia flames.

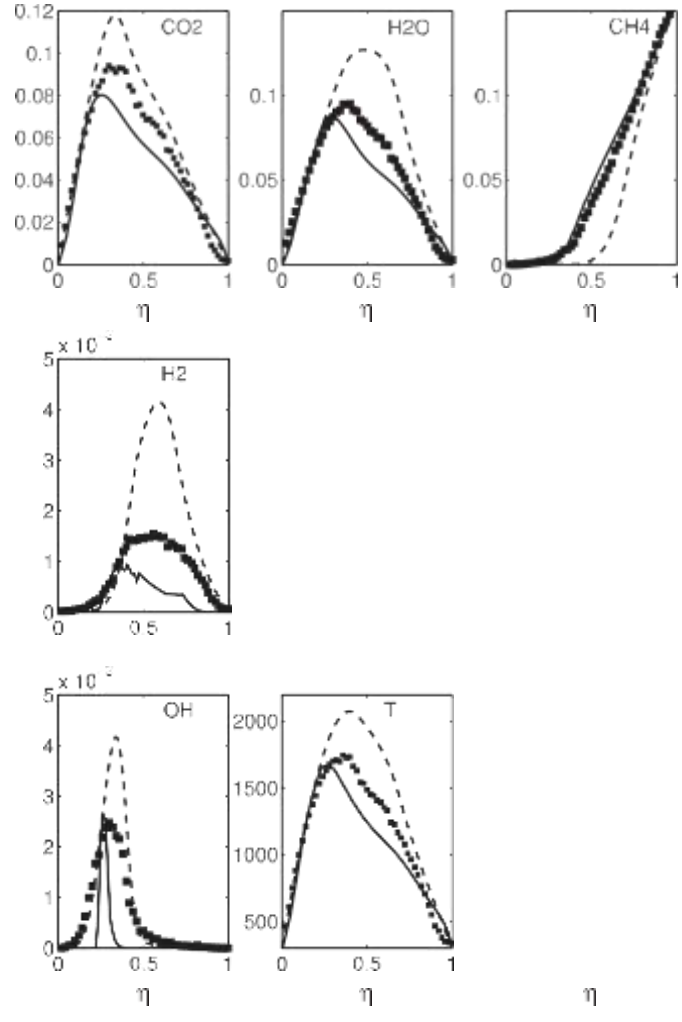

Fig.18.CSE(solidlines)andCMC (dashed lines) condtional temperature andspeciesprofilescomparedtotheexperimentaldata[40](symbols)at*y*/*D*=7.5forthe SandiaEflame.

needed to record extinction [55]. By causing fluctuations in the jet's speed, inert profiles in the fuel jet may be convected radially outward. When added to the extinction brought on by a high scalar dissipation rate, this phenomenon becomes impossible to reverse. In contrast, as shown in [55], the extinction process through the radially outward convective transport is not present when burning flamelets are provided as a boundary condition in the fuel jet. Even with the mixed boundary condition, with inert boundary conditions in the fuel jet, RANS is unable to recreate the velocity fluctuations, and the average radially outward convection is insufficient to adequately depict the extinction process. In light of this, it is clear that the present research cannot make reliable predictions about the end of the world.

In contrast, CSE is rather accurate in capturing the cooling effect of increasing jet velocity. When comparing Flame D with Flame E, the current research finds that Flame E has lower peak values for temperature and species. This may be seen as a result of the inversion process creating a link between the unconditional and conditional mass fractions. The unconditional mass fractions of CO2 and H2O will fall as the jet speed rises. The decreasing conditional mass fractions reflect the time required for the change in the unconditional mass fractions. However, for OH and H2 with levels below the limits, this drop is too pro- nounced.

Both models failed to generate reliable predictions for Sandia flame F using the present conditions specified in Section 4. As was shown above for Flame E, the inaccurate prediction of extinction in CMC results from the use of RANS and the boundary condition imposed. Additional increases in jet velocity caused blow-off in the case of CSE. Given that the CSE forecasts underpredict the species mass fractions and temperature for Flame E, this pattern makes sense. Species mass fractions and temperature drop as velocity increases, and this is what causes a blow-off.

Computational Time Comparison

Currently, the CSE code has not been optimized in any way. For matrix inversions of a comparable size, recent research by Hong and Bushe [71] has shown that switching from the LU decomposition matrix solver utilized in the present work to the LSQR solver may result in a 19–55% reduction in computing time. On the other hand, the present CMC code is the result of a more protracted period of development by groups at Ghent University [15,16] and the University of Cambridge [12,17,18].

It has been determined that the CSE submodel alone accounts for over 85% of the computational time in RANS-CSE. Matrix inversion, extraction of conditional species and reaction rate data from TGLDM tables, and computation of unconditional species and reaction rates are all part of the CSE submodel. 15% of the CPU time is spent calculating transport equations for pressure, velocity, mixture fraction, mixture fraction variance, and mass fraction of CO2 and H2O. The CSE combustion model takes around 7.6 seconds for a single timestep when run on a cluster of Intel Xeon E5-2680v3 processors operating at 2.5 GHz utilizing a single processing core. The CMC subroutines account for almost all of the CPU time in the RANS/CMC computations. Single timesteps for CMC on the same cluster operating on five cores take around 3.6 seconds, with a total computational resource need of about 18 CPU seconds. In the current computational cost, the CPU time required to build the TGLDM tables is not accounted for. CSE looks to be quicker than CMC for the present calculations based on CPU time, without any optimization and including the time required to generate the chemical tables. Furthermore, based on the time needed to determine the conditional average of a single species, a rough estimate of the computing time necessary for CSE without optimization or tabular chemistry is provided. As used in CSE, this is the sum of the times it takes to do the inversion and to solve the unconditional species transport equation. In the current investigation, a single conditional average requires around 0.32 seconds of CPU time to calculate. On the other hand, a single CMC transport equation can be solved in around 0.12 CPU seconds. Therefore, CSE is about 2.6 times slower than CMC in calculating the conditional av- erages in the absence of

toimplement a new chemical mechanism, new tables must be predicting the minor species at some locations. Further,theinclusionofcomplexfuelsintotheTGLDMtablesrequir esspecial considerations to correctly construct the boundaries of themanifold. Specifically, a method for accurately estimating the massfractionofminorspeciesandmulti-componentfuelsalongtheboundary of the TGLDM is required. In the current study, CMCproducessmootherconditionalprofilesfortheminorspeciesa tallaxiallocations.CSEyieldsprofilesfortheconditionalaverages of certain inconspicuous species, whose roughness results from the fact that one does not need to rely on tabular chemistry in order to determine their composition.

mean values for the rare species derived via the inversion technique. Practicing chemistry requires pretabulating it for computational efficiency. Many CSEs, most notably RANS, offer tabulations of chemical data. However, CMC is different since it automatically solves the transport equations.
CMC and CSE simulations need identical caution throughout their respective startup phases. A properly burning flame in CMC requires precise boundary conditions for the conditional averages. Selecting the initial conditional profiles for YCO2 and YH2 O in CSE involves some knowledge and expertise to guarantee that YCO2 and YH2 O reach adequate levels to continue combustion. Blow off may occur if the ensemble's optimization and chemistry tabulation. In CSE, without tabular chemistry, this data allows for a ballpark approximation of the calculation time required. A CSE model without tabular chemistry would need about 21.8 CPU seconds, which is 20% greater than CMC assuming the only com- putational time difference between the two programs was the computation of the conditional averages.

Comparison of the CMC and CSE methodologies: 5.2.

Given the identical numerical setup, sections 5.1.1-5.1.5 showed that CMC and CSE could generate predictions that were in excellent agreement with each other. The advantages and disadvantages of each method used in the present research are discussed below.

CMC calls for far more intricate boundary conditions to be put up correctly than CSE does. The mixture percent, its variance, and the mass fraction of YCO2 and YH2 O are all necessary boundary conditions in CSE, and they may be easily computed from experimental data. Comparatively, CMC necessitates boundary conditions for mixture fraction, its variance, conditional temperature, and conditional mass fraction of all species. As a result, these conditional profiles have to be estimated rather than acquired directly from the experimental data.

As a result of how the CMC is now implemented, incorporating new chemical schemes is simpler. Substituting one chemical mechanism for another has no effect on the CMC recipe. In addition, CMC can simulate intricate fuel composi-without any kind of special treatment. The TGLDM method is used for tabulation of chemical data in the current CSE model. Thus

,Table1

StrengthdescribedinSection5.4.Levelsofdifficultytoaccomplisheachtask:low (easy),mediumandhigh(difficult).

Task	CMC	CSE
Boundaryconditionsetup	High	Low
Inclusionofchemistry	Low	Medium
Initialization	Medium	Medium
Meshforconditionalaverages	Low	High
Expandingtomorecomplexcases		
Extinction	High	High
Differentialdiffusion	High	High
Soot	High	High
Radiation	Medium	Medium
Extensiontoothercombustionregimes	High	Medium

initial response rates are too low, which can happen if the conditional profiles for the conditions are not chosen carefully. Selecting the CSE ensem- bles, which is presently done with a priori knowledge of the flame, is more difficult than generating the CMC grid. Sophisticated ways to choose the best en-semble to use have been studied as of late [72]. Since CSE needs the ensembles to be big enough to enable sufficient information for the inversion process, they cannot be refined to the same degree as CMC ensembles.
The CMC technique has the potential to accurately foresee the occurrence of both extinction and revival. The precision of the forecasts, however, is sensitive to a number of aspects that need specific attention: the conditional scalar dissipation modeling [19,55]; transport in the cross stream direction; and the selection of CMC boundary condition. The computational cost rises when dealing with situations that need a CMC formulation in several dimensions. Insightful knowledge of the

flame may be achieved by solving CMC transport equations. Some data on flame stabilization [15] and extinction [19] processes may be acquired, for instance, by analyzing the contributions of the various components in the CMC equation. These findings suggest that CSE is successful in representing certain features of extinction. The present research shows that a lot of work has to be done before CSE can reliably anticipate extinction and re-ignition. In all likelihood, LES with a double-conditioned CSE formulation is required, although this has not yet been performed.

One of CMC's key features in terms of model formulation is that information is transferred across CMC cells through the transport equation, and differential diffusion may be added to the underlying conditioned transport equations. However, including differential diffusion into CMC is still not simple [73]. The conditional averages in CSE are computed separately from one another, and the model does not account for the diffusion of the conditional averages. In order to implement differential diffusion in CSE, the chemical tables would need to be updated to reflect this concept. It is anticipated that incorporating soot or radiation into CMC [13] or CSE [31] would provide a similarly formidable challenge. Premixed, partly, and doubly conditioned formulations all follow the same general structure, which is a key benefit of the CSE method.form as that of non-premixed CSE. The CMC approach cannot be easily extended to a doubly conditioned formulation as additionalunclosed terms appear which require closure. For clarity, a summaryofthosestrengthsandweaknessesofeachcombustionmodelis given in Table 1, with different levels of complexity from low(easy),mediumtohigh(difficult).

4. Conclusions

Both CMC and CSE are studied here by comparing the Sandia flames side by side. To reduce the likelihood of inconsistencies between the two models, the identical CFD numerical techniques, mesh, and boundary conditions are utilized for both sets of simulations. The results of CMC and CSE are compared to extensive experimental data.

Near the nozzle exit, the turbulent flow and mixing fields in the CMC and CSE simulations are consistent with experimental results. Away from the centerline and farther downstream, there are noticeable inconsistencies between the CMC and CSE profiles, as well as with the experimental data. Near the nozzle, the mixture fraction rms exhibits the same trends and overall shape for both CMC and CSE models. In the downstream region, the rms values of the mixture fractions are less in the CMC findings compared to the CSE and the experimental data. The anticipated temperature profiles from CMC and CSE are different, which accounts for the discrepancy in forecasts.

For lean mixtures, the conditional mass fractions predicted by CMC and CSE for the principal species are in excellent agreement with actual data downstream of the nozzle, with the CMC and CSE findings frequently being indistinguishable. The conditional mass fractions of CH4 and H2O in fuel-rich mixes are underpredicted and overestimated, respectively, at particular axial sites. The main features of the experimental profiles are recapitulated by the CMC and CSE conditional mass fractions of the minor species and conditional temperature. Larger discrepancies between CMC and CSE are seen for the minor species, and they are due to the various approaches used to determine the chemical source-term (calculated during the simula- tion in CMC and retrieved from pre-tabulated chemistry tables in CSE). Large gra- dients at the boundary in the TGLDM tables lead to bigger deviations in the CSE conditional mass fractions of H2 and OH in fuel-rich mixes. Differences between CMC and CSE at the nozzle exit are explained by the use of CMC boundary conditions.

In both CMC and CSE simulations, the same general tendencies are reproduced from the Favre-averaged profiles, and equivalent quality simulation results are achieved. It has been predicted by CMC and CSE that the flame would spread outward from the nozzle. The volume and broad patterns of the downstream are accurately reproduced by CMC and CSE. profiles of the main temperature and species groups. For the minor species derived via CMC and CSE, the disparities between the experimental data and Favre-averaged profiles are higher than for the conditional profiles.

The jet velocity, turbulence-chemistry interactions, and local extinction are all more prominent in Sandia flame E, making the choice of combustion model more crucial. The CSE simulations mimic the higher level of local extinction, which is observable in lower temperatures and large species mass fractions, but to an unrealistic degree. There is a disconnect between this tendency and how CMC is currently implemented. Only with LES is it possible to account for the velocity fluctuations and implement more advanced boundary conditions, both of which are necessary for achieving optimal results with CMC. As a corollary, conditional scalar dissipation modeling is crucial. Both models failed to successfully simulate Sandia flame F at the present conditions.

A look at the computing time needed for each combustion model reveals that CMC takes higher computational resources for the present flame. Further, some of the benefits and drawbacks of each combustion model are discussed. The CSE method is easier to use when it comes to defining the boundary conditions, while the CMC method is more convenient when it comes to setting up the mesh needed for the conditional averages.

References

Phys. Fluid A: Fluid Dyn. 25 (1990) 327-334, cites the work of [1] A. Klimenko, Multicomponent diffusion of different admixtures in turbulent flow.

Phys. Fluid A: Fluid Dyn. 5 (1993) 436–444. [2] R. Bilger, Conditional moment closure for turbulent reactive flow.

For example, see [3]W.K. Bushe and H. Steiner, Conditional moment closure for large eddy modeling of non-premixed turbulent reacting flows, Phys. Fluids 11 (1999) 1896-1906.

Conditional moment closure for turbulent combustion, Prog. Energy Combust. Sci. 25 (6) (1999) 595-687 [4], A. Klimenko, R. Bilger.

Nitric oxide generation in dilute hydro-gen jet flames: Separation of the impacts of radiation and turbulence-chemistry submodels, Combust. Flame 117 (1999) 4-31, R. Barlow, N. Smith, J.-Y. Chen, and R. Bilger.

Combust. Flame 152 (2007) 282-286; S. Sreedhara, Y. Lee, K.Y. Huh, D. Ahn, Comparison of submodels for conditional velocity and scalar dissipation in CMC modeling of piloted jet and bluff-body flames.

(7) M.R. Roomina and R.W. Bilger, "Conditional moment closure (CMC) predictions of a turbulent methane-air jet flame," Combust. Flame 125 (2001) 1176-1195.

Soot production in turbulent nonpremixed ethylene flames: a conditional moment closure prediction (Yunardi, R. Woolley, M. Fairweather, Combust. Flame 152, 2008, pp. 360-376).

Phys. Fluids 10 (1998) 1246-1248; E. Mastorakos and R.W. Bilger, Second-order conditional moment closure for the autoignition of turbulent flows.

Autoignition research using a conditional moment closure method and an inhomogeneous turbulent mixing model, Combust. Flame 157, 1467-1483 (2010) [10].

To cite: [11] M. Cleary, J. Kent, Conditional moment closure modeling of species distributions during hood fires, Fire & Flame 143:357-368 (2005).

Researchers G. Borghesi, E. Mastorakos, C.B. Devaud, and R. Bilger Conditions for igniting in sprays, including modeling of evaporation effects, In Combust. Theor. Model. 15 (2011), pages 725-752.

To cite this entry: [13] M. Bolla, Y. Wright, K. Boulouchos, G. Borghesi, E. Mastorakos, The conditional moment closure method is used to a model of soot production in n-heptane sprays in a diesel engine. 185, 7, 676–793 (2013), Combust. Science & Technology.

Reference: [14] S. Navarro-Martinez and A. Kronenburg, "LES-CMC simulations of a raised methane flame," Proc. Combust. Inst. 32 (2009), pp. 1509-1516.

Simulation of hydrogen auto-ignition in a turbulent co-flow of hot air using the LES and CMC technique, Flow Turb. Combust. 86 (2011)

689-710, I. Stankovic', A. Triantafyllidis, E. Mastorakos, C. Lacor, B. Merci.

Based on the work of I. Stankovic', E. Mastorakos, B. Merci, and LES-CMC Hydrogen in a hot, turbulent air co-flow was simulated using Flow Turb to explore the many auto-ignition regimes that may occur. Combustion 90 (2013):583-604.

[17] E. Mastorakos, Large eddy simulations of a non-premixed bluff-body methane flame with conditional moment closure, A. Triantafyllidis and R. Eggels, Proc. Burning Flame 156 (12): 2328–2345 (2009).

[18]

An Experimental Study of the Critical Mass Combustion (LES/CMC) of Blow-Off in a Liquid-Fueled Swirl Burner, A. Tyliszczak, D. Cavaliere, and E. Mastorakos, Chemical Engineering Science, Flow, Turbulence, and Combustion, 92, 237-267 (2014).

Numerical modeling of oxyfuel jet flames using unstructured LES-CMC, Proc. Combust. Inst. 35 (2015) 1207-1214, A. Garmory and E. Mastorakos.

The conditional moment closure model [20] A. Kronenburg, E. Mastorakos, in: T. Echekki, E. Mastorakos (Eds.), Turbulent Combustion Modelling Advances, New Trends and Perspectives, Springer (2011), pp. 91-117.

Conditional moment closure for turbulent premixed flames, Combust. Sci. Technol. 184 (2012) 1743-1767, S. Amzin, N. Swaminathan, J. Rogerson, J. Kent.

Phys. Fluids 16 (2004) 2640-2648 cites the work of [22] A. Kronenburg, Double conditioning of reactive scalar transport equations in turbulent nonpremixed flames.

According to [23] "A. Kronenburg and M. Kostka, Modeling extinction and reignition in turbulent flames," Combust. Flame 143 (2005) 342-356.

According to [24] Laminar flamelet decomposition for conditional source-term estimate, W.K. Bushe and H. Steiner, Phys. Fluids 15, 1564-1575 (2003).

The ignition delay of turbulent methane jets may be predicted using conditional source-term estimate [25] (R.W. Grout, W.K. Bushe, and C. Blair). Combust. Theor. Model. 11 (2007) 1009-1028.

Reference: [26] M.M. Salehi, W.K. Bushe, K.J. Daun RANS simulation of turbulent premixed flames, based on an assumed PDF model, 16 (2012), pp. 301-320 in Combust. Theor. Model.

[27]John Labahn, Claude Devaud, The use of conditional source term estimation (CSE) on a non-premixed turbulent flame is explored. 17(5), 960-982 (Combust. Theor. Model).

[28]Wang, Jian-Hua, Bushe, William Conditional source-term estimation using a low-dimensional manifold derived from a trajectory for simulating a turbulent non-premixed flame, Proc. Combust. Inst. 31 (2007) 1701-1709.

[29]Transient turbulent methane jet igni- tion and combustion simulation under engine-relevant circumstances utilizing conditional source-term estimate with precise chemistry, J. Huang and W. Bushe, ACS Applied Energy Materials and Energy Systems, 2018. 11:977–1008 (2007), Combust. Theor. Model.

[30]

Conditional source-term estimation (CSE) applied to two turbulent non-premixed methanol flames, S. Lee and C. Devaud, Applied Plasma Spectroscopy and Flame Dynamics, 58, pp. The Combustion Theory and Modeling 20 (5):765-797 (2016).

Species and temperature forecasts in a semi-industrial MILD furnace using a non-adiabatic conditional source-term estimate for-mulation, Combust. theor. Model. (2017) 1-21, doi:10.1080/13647830.2016. 1249960, J. Labahn and C. Devaud (in press).

RANS simulation of a turbulent premixed bluff body flame using conditional source-term estimation, [32] D. Dovizio, M. Salehi, and C. Devaud. Burning Theory and Multiscale Modeling 17 (2013) 935-959.

According to [33] N. Shahbazian, M. Salehi, C. Groth, O. Gülder, and W. Bushe The effectiveness of a conditional source term estimation model for LES of turbulent premixed flames in the narrow reaction zone regime, Proc. Combust. Inst. 35 (3), 1367-1375 (2015).

Specifically: [34] J. Labahn, D. Dovizio, C. Devaud, Conditional source-term estimate in a numerical model of the Delft-Jet-in-Hot-Coflow (DJHC) flame, Proceedings of the Combustion Institute, Volume 35, Issue 3, Pages 3547–3555, 2015.

Based on the work of J. Labahn and C. Devaud, "Large eddy simulations (LES) with conditional source-term estimation (CSE) applied to two Delft-Jet-in-Hot-Coflow (DJHC) flames," [35] Flammable, Combustion 154 (2016) 68-84.

Doubly conditional source-term estimation (DCSE) applied to a succession of lifted turbulent jet flames in cold air, [36] D. Dovizio, J. Labahn, and C. Devaud. Embers, Flame 162(5) (2015) 1976-1986 (2015).

According to [37] (D. Dovizio, A. Debbagh, C. Devaud, RANS Simulations of a Sequence of Turbulent v-Shaped Flames Using Conditional Source-Term Estimation), Flow, Turbulence, and Combustion, 96, 891–919. (2016).

Doubly conditional source-term estimate (DCSE) for the modeling of turbulent stratified v-shaped flame, Combust. Flame 172 (2016) 79-93, Dovizio, C. Devaud.

Based on the work of J. Labahn, C. Devaud, T. Sipkens, and K. Daun [39], Combust. Theor. Model 18 (3) (2014) 474-499, Inverse analysis and regularization in conditional source-term estimation modeling.

According to [40] R. Barlow and J. Frank, "Effects of turbulence on species mass fractions in methane/air jet flames," Proc. Comb. Inst. 27 (1998) 1087-1095.

Large-eddy simulation of a turbulent piloted methane/air diffusion flame (Sandia flame D), Phys. Fluids 12 (10) (2000) 2541-2554, H. Pitsch, H. Steiner.

Combust. Flame 124 (2001) 444-465, P. Coelho and N. Peters, "Unsteady modeling of a piloted methane/air jet flame based on the Eulerian particle flamelet model."

Nonpremixed turbulent flames: prediction of extinction and reignition using a flamelet/progress variable model, [43] M. Ihme and H. Pitsch. Applications of Sandia flame types D and E in LES, Combust. Flame 155 (2008) 90-107.

R. Mustata, L. Valio, C. Jiménez, W. Jones, and S. Bondi [44] Using the Eulerian Monte Carlo field approach with a probability density function to simulate a turbulent piloted methane/air diffusion flame (Sandia D), Combust. Flame 145 (2006) 88-104.

K. Xiao, D. Schmidt, and U. Maas [45] Using a probability density function approach, the authors of Proc. Comb. Inst. 28 (2000) 157-165 examine the local flame structures in a piloted jet diffusion flame.

[46]

F. Jaberi, S. Pope, M. Sheikh, T. Drozda, P. Givi, The turbulent nonpremixed piloted methane jet flame (Sandia Flame D) was modeled using large eddies and was published in the Proceedings of the Combustion Institute 30 (2000) 549-556.

Large-eddy simulation of non-premixed turbulent combustion using a progress-variable technique [47], R. Lindstedt, S. Louloudi, E. Váos, Proc. Comb. Inst. 28 (2000) 149-156.

pdf estimates of turbulent nonpremixed flames with local extinction, Combust. Flame 123 (2000) 281-307, J. Xu.